

# Driving Referring Video Object Segmentation with Vision-Language Pre-trained Models

Zikun Zhou, Wentao Xiong, Li Zhou, Xin Li,  
Zhenyu He, *Senior Member, IEEE* Yaowei Wang, *Member, IEEE*,

**Abstract**—The crux of Referring Video Object Segmentation (RVOS) lies in modeling dense text-video relations to associate abstract linguistic concepts with dynamic visual contents at pixel-level. Current RVOS methods typically use vision and language models pre-trained independently as backbones. As images and texts are mapped to uncoupled feature spaces, they face the arduous task of learning Vision-Language (VL) relation modeling from scratch. Witnessing the success of Vision-Language Pre-trained (VLP) models, we propose to learn relation modeling for RVOS based on their aligned VL feature space. Nevertheless, transferring VLP models to RVOS is a deceptively challenging task due to the substantial gap between the pre-training task (image/region-level prediction) and the RVOS task (pixel-level prediction in videos). In this work, we introduce a framework named VLP-RVOS to address this transfer challenge. We first propose a temporal-aware prompt-tuning method, which not only adapts pre-trained representations for pixel-level prediction but also empowers the vision encoder to model temporal clues. We further propose to perform multi-stage VL relation modeling while and after feature extraction for comprehensive VL understanding. Besides, we customize a cube-frame attention mechanism for spatial-temporal reasoning. Extensive experiments demonstrate that our method outperforms state-of-the-art algorithms and exhibits strong generalization abilities.

**Index Terms**—Referring video object segmentation, vision-language pre-trained models, temporal modeling, vision-language relation modeling

## I. INTRODUCTION

**R**EFERRING Video Object Segmentation (RVOS) aims to segment the target object in a video according to the referring expression. It has a wide range of applications, including language-based robot controlling [1], [2], augmented reality [3], and video editing [4], [5]. As language descriptions inherently exhibit flexibility and diversity, RVOS necessitates comprehensive Vision-Language (VL) understanding abilities to accurately discover and segment the referred target.

The crux of RVOS lies in modeling dense text-video relations to associate the diverse yet abstract linguistic concepts with dynamic visual contents at pixel-level. Massive endeavors [3], [6], [7] have been made for this purpose in the RVOS

Zikun Zhou and Zhenyu He are with the School of Computer Science and Technology, Harbin Institute of Technology, Shenzhen, China, and also with the Peng Cheng Laboratory, Shenzhen, China (e-mail: zhouzikun-hit@gmail.com; zhenyuhe@hit.edu.cn).

Wentao Xiong and Li Zhou are with the School of Computer Science and Technology, Harbin Institute of Technology, Shenzhen, China (e-mail: 21s151086@stu.hit.edu.cn; lizhou.hit@gmail.com).

Xin Li and Yaowei Wang are with the Peng Cheng Laboratory, Shenzhen, China. Yaowei Wang is also with the School of Computer Science and Technology, Harbin Institute of Technology, Shenzhen, China (e-mail: xinlihitsz@gmail.com; wangyw@pcl.ac.cn) Zikun Zhou and Wentao Xiong contribute equally to this work.

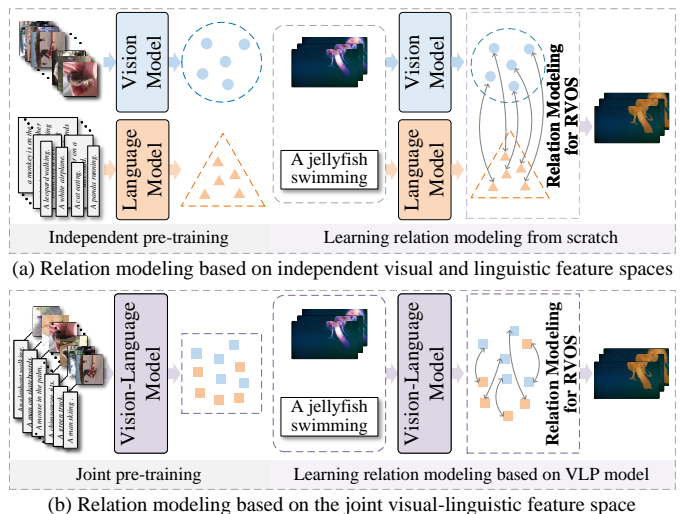


Fig. 1. Two paradigms of learning dense text-video relation modeling for RVOS. Compared with learning from scratch, learning such a relation modeling ability based on the aligned VL feature space is more accessible and derives better performance.

community. Existing RVOS algorithms [3], [6], [7] typically build relation modeling components on independently pre-trained vision and language backbones, including ResNet [8], Video-Swin [9], and RoBERTa [10]. Such a paradigm for learning relation modeling can be summarized as Figure 1 (a). As the backbones map input images and texts into decoupled feature spaces, these algorithms face the challenge of learning VL relation modeling for RVOS from scratch. Although resorting to sophisticated relation modeling mechanisms, they struggle to understand complicated descriptions and videos.

Recently, Vision-Language Pre-trained (VLP) models, such as CLIP [11] and VLMO [12], which can map images and texts into aligned feature space, have drawn much attention. VLP models have played a pivotal role in advancing various tasks, such as zero-shot classification [11] and referring image segmentation [13], [14]. Nevertheless, the application of VLP models in RVOS remains unexplored. In light of this, we seek to unleash the power of VLP models by transferring them to RVOS, allowing us to learn relation modeling for RVOS based on the aligned VL features instead of from scratch, as shown in Figure 1 (b). Compared with the transfer to image segmentation [13], [15], the transfer to RVOS poses a more formidable challenge due to the substantial gap between the pre-training task (image/region-level prediction) and the RVOS task (pixel-level prediction in videos). Particularly, the transfer

to RVOS demands not only adapting the image/region-level representation for pixel-level prediction, but also empowering the pre-trained model with temporal modeling ability. As shown in Figure 2, a model using CLIP [11] without temporal modeling loses the target person when the blue jeans disappear in the 140<sup>th</sup> frame.

In this work, we introduce a framework called VLP-RVOS, with the goal of transferring the knowledge of VLP models to learn robust spatial-temporal and vision-language relation modeling for RVOS. The primary challenge is to learn the task-specific prior knowledge from limited video data without forgetting the pre-trained knowledge of vision-language association. To address the issue, we resort to parameter-efficient prompt-tuning, which keeps the VLP model frozen to retain the pre-trained knowledge, instead of fine-tuning it. In particular, we propose a temporal-aware VL prompt-tuning method, which not only adapts the pre-trained VL features for pixel-level prediction but also empowers the vision encoder to capture temporal clues. For comprehensive VL understanding, our framework incorporates multi-stage VL relation modeling, including 1) introducing the linguistic reference guidance during visual feature extraction, 2) fusing the deep VL features after feature extraction, and 3) VL relation modeling during spatial-temporal reasoning. Besides, we tailor a cube-frame attention mechanism to efficiently and effectively perform spatial-temporal reasoning for RVOS.

Extensive experiments on four benchmarks [16]–[18] show that VLP-RVOS outperforms state-of-the-art methods. Figure 3 illustrates the comparison on Ref-DAVIS17 [18] in learnable param and  $\mathcal{J}\&\mathcal{F}$ . The favorable performance demonstrates that our framework effectively unleashes the power of VLP to RVOS. Our contributions can be concluded as:

- We introduce the VLP-RVOS framework, facilitating the transfer of VLP models to RVOS; it enables us to learn relation modeling for RVOS from aligned VL feature space instead of from scratch.
- We propose a temporal-aware prompt-tuning method, which not only adapts pre-trained features for pixel prediction but also enables the vision encoder to capture temporal clues.
- We propose a multi-stage VL relation modeling scheme for comprehensive VL understanding, and tailor a cube-frame attention mechanism for efficient and effective spatial-temporal reasoning.

## II. RELATED WORK

**Referring video object segmentation.** The main challenge of RVOS lies in modeling the dense text-video relation. Numerous sophisticated VL relation modeling mechanisms [3], [7], [19]–[25] have been proposed to address the challenge. For example, VT-Capsule [19] uses capsules to model VL representations and fuses the visual and linguistic capsules with a routing mechanism to segment the target. Recently, many RVOS algorithms [3], [4], [6], [7], [26]–[28] resort to attention-based methods for VL or spatial-temporal relation modeling. Specifically, LBDT [4] proposes a language-bridged duplex transfer module to accomplish spatial-temporal interaction. MTTR [6] and ReferFormer [7] introduce the DETR [29]

*Query: a person wearing blue jeans is at the left of a brown kangaroo sitting on the green grass.*

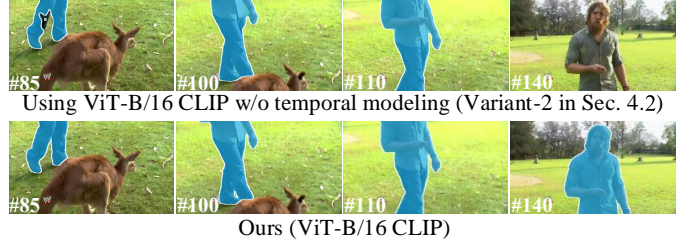


Fig. 2. **Comparison between using ViT-B/16 CLIP w/o and w/ temporal modeling.** When the blue jeans disappear from view in the 140<sup>th</sup> frame, our method can still understand that the person is the referred target according to the temporal clue, while the variant without temporal modeling cannot.

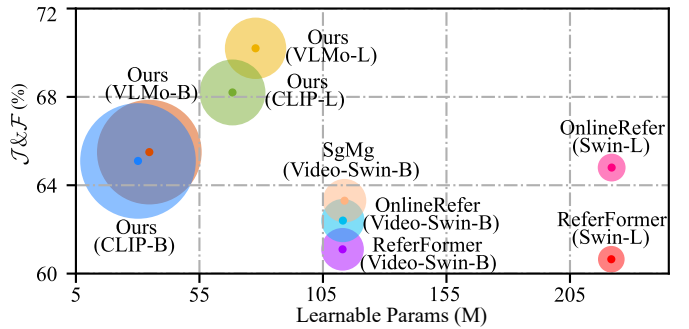


Fig. 3. **Comparison with state-of-the-art algorithms on Ref-DAVIS17 [18].** We visualize  $\mathcal{J}\&\mathcal{F}$  w.r.t. the learnable params of different methods. Note that we freeze the VLP model. The circle size indicates the ratio of  $\mathcal{J}\&\mathcal{F}$  to the learnable params.

architecture to RVOS and use language as queries to attend to the referred target. HTML [30] and TempCD [31] improve the temporal modeling ability by hybrid temporal-scale learning and temporal collection and distribution, respectively, which achieve promising RVOS performance.

Nevertheless, these RVOS algorithms construct the relation modeling components on independently pre-trained vision and language backbones and learn relation modeling from scratch, which is a tough learning task. Unlike these methods, we propose to transfer the powerful VLP model to RVOS, allowing us to learn relation modeling for RVOS from a joint VL feature space instead of from scratch.

**Referring image segmentation.** Referring Image Segmentation (RIS) is closely related to RVOS, whose goal is to segment the target object described by the referring expression in a static image. Similar to existing RVOS algorithms, numerous RIS approaches [32]–[35] adopt a pipeline of first extracting the visual and linguistic features and then modeling the cross-modality relation based on the unimodal representations for image mask prediction. Most of these algorithms [33]–[37] resort to independently pre-trained vision and language backbones and learn VL relation modeling from scratch. A few methods [13], [14], [38] build the RIS framework on top of the vision-language pre-trained model, CLIP. Compared with the CLIP-based RIS approaches, transferring VLP models to RVOS is much more challenging due to the larger gap between the pre-training task and the RVOS task.

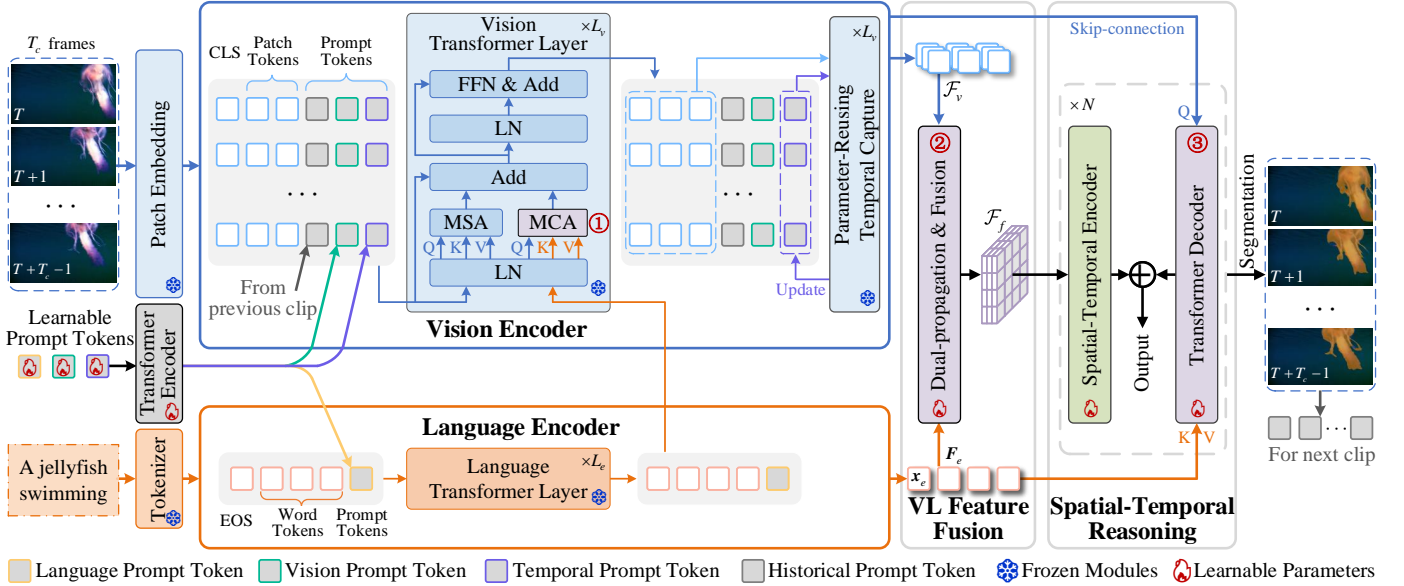


Fig. 4. **Overall architecture of VLP-RVOS**, which processes long videos clip-by-clip. The prompt tokens are first appended to the input VL tokens. Then the vision encoder extracts video features with the guidance of learnable vision/temporal prompts and historical prompts conditioned on the previous clip. The language encoder, tuned by learnable language prompts, extracts linguistic features. VL feature fusion and spatial-temporal reasoning modules associate linguistic concepts with corresponding dynamic visual contents. A segmentation head is used for final target segmentation. ①, ② and ③ mark the three VL relation modeling stages. MSA/MCA denotes multi-head self/cross-attention. LN is layer normalization.  $\oplus$  is element-wise summation.

**Vision-language pre-trained models.** Recently, VLP models [11], [12], [39]–[41], learning multi-modality representation on large-scale image-text pairs, have attracted much attention. They typically adopt a dual-stream [11], [39], [42]–[44] or single-stream [40], [41] encoder structure to extract the visual and linguistic features and align them via cross-modality interaction. VLP models have driven the progress of various downstream tasks, such as image-text retrieval [11], [12], [40], referring image segmentation [13], [14], [38], and open-vocabulary detection [45]. Nevertheless, the exploitation of VLP models for RVOS has not been explored. In this paper, we try to overcome the discrepancy between the pre-training and RVOS tasks and take a step towards transferring the powerful VLP models to RVOS.

**Prompt-tuning.** Prompting was proposed in NLP [46]–[48] to generate task-specific instructions for the language model to obtain desired outputs. Recently, prompt-tuning has been widely explored in vision and multi-modal problems to efficiently adapt the pre-trained model to downstream tasks, including image/video recognition [49]–[51], image segmentation [14], [52], video-text retrieval [53], and domain adaptation [54]. Nevertheless, prompt-tuning has not been explored in the RVOS area, which requires pixel-level video-text understanding and is different from the above-mentioned tasks. In this work, we explore adapting the pre-trained VL representation to RVOS via prompt-tuning.

### III. VLP-RVOS

Figure 4 illustrates the architecture of VLP-RVOS, which mainly consists of the VLP model, the VL Feature Fusion (VLFF) module, and the Spatial-Temporal Reasoning (STR) module. To learn task-specific knowledge from limited video

data without forgetting pre-trained knowledge, we opt for the parameter-efficient prompt-tuning method, instead of fine-tuning the VLP model in our framework, which poses the risk of hurting the generalization ability. Specifically, we design a temporal-aware VL prompt-tuning method to enable the vision encoder to capture the temporal clue for video understanding.

For comprehensive VL understanding, VLP-RVOS is designed to conduct three-stage VL relation modeling: 1) We introduce additional Multi-head Cross-Attention (MCA) operations into the vision encoder to exploit the additional linguistic reference guidance for feature extraction. 2) We employ the VLFF module to fuse deep VL features for associating high-level visual semantics with abstract linguistic concepts. 3) We perform VL relation modeling between linguistic features and shallow visual features in the STR module; the goal is to introduce low-level semantic guidance for understanding the motions or appearance variations described in the text. The three stages are marked by the red numbers in Figure 4. Subsequently, we delve into the specifics of VLP-RVOS.

#### A. Vision-Language (VL) encoders

**Vision encoder.** Given a clip  $\mathcal{V} = \{\mathbf{I}^t\}_{t=T}^{T+T_c-1}$  with  $T_c$  frames from a long video, where  $T$  is the index of its beginning frame, the vision encoder (e.g., ViT-B/16 [55] of CLIP) extracts visual features for each frame with the tuning of prompt tokens. We first bracket the patch embeddings of each frame with a CLS token and the prompt tokens, then feed them into the transformer layers for feature extraction. We further process the visual feature with a projection layer to align its dimension  $C_v$  with that of the linguistic feature  $C_e$  for dimension consistency. The resulting video feature is denoted by  $\mathcal{F}_v = \{\mathbf{F}_v^t \in \mathbb{R}^{(N_v+1) \times C_e}\}_{t=T}^{T+T_c-1}$ , where  $\mathbf{F}_v^t$  is the feature

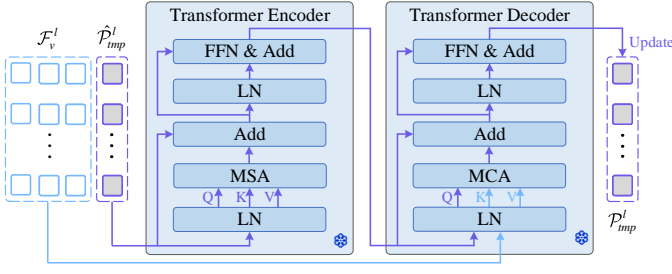


Fig. 5. **Illustration of our Parameter-Reusing Temporal Capture module.** It reuses each transformer layer in the VLP model as the encoder and decoder to capture the temporal clue.

of the  $t$ -th frame and  $N_v$  is the number of patch embeddings per frame. Note the output tokens corresponding to prompts are dropped in  $\mathcal{F}_v$ .

**Language encoder.** Given a referring expression  $\mathcal{E} = \{\mathcal{W}_n\}_{n=0}^{N_w-1}$  with  $N_w$  words, we first tokenize each word and bracket the word embedding sequence with an SOS token and an EOS token. Then the language encoder (*e.g.*, the modified Transformer [56] of CLIP), tuned by learnable language prompts, processes this sequence to extract the linguistic feature  $\mathbf{F}_e \in \mathbb{R}^{N_e \times C_e}$ . Herein  $N_e$  is the number of linguistic feature tokens. The token in  $\mathbf{F}_e$  corresponding to EOS is the global representation of  $\mathcal{E}$ , and we denote it by  $x_e$ .

### B. Temporal-aware VL prompt-tuning

To preserve pre-trained knowledge, we opt for prompt-tuning to adapt the VLP model to RVOS, which keeps the VLP model frozen and learns a small number of prompt tokens. Particularly, we design a temporal-aware VL prompt-tuning method to adapt the VLP model for pixel-level prediction and enable it to capture temporal clues. Next, we elaborate on the prompt-tuning method.

1) *Temporal-aware vision prompt-tuning:* Prompt-tuning on the vision encoder has two objectives: 1) adapting the visual representation pre-trained for image/region-level prediction to pixel prediction; 2) empowering the vision encoder to capture and exploit the temporal clue in videos. To this end, we introduce three types of prompt tokens: the vision prompt, the temporal prompt, and the historical prompt.

**Vision prompt.** The vision prompt tokens  $\mathbf{P}_v \in \mathbb{R}^{M_v \times C_v}$  are introduced to adapt the pre-trained visual representation for pixel prediction. Technically, they are randomly initialized learnable vectors. We adopt a deep prompt-tuning strategy on the vision decoder to provide additional learning capacity for each transformer layer. Specifically, we divide the  $M_v$  vision prompt tokens into  $L_v$  groups, each containing  $m_v = M_v/L_v$  prompt tokens. These groups are then appended to the patch tokens of each vision transformer layer. Herein  $L_v$  is the number of vision transformer layers. All frames share the same prompt tokens in each layer.

**Temporal prompt.** The *temporal prompt* tokens  $\mathbf{P}_{tmp} \in \mathbb{R}^{m_{tmp} \times C_v}$  are used as carriers to capture and spread the temporal clue in the input video clip. Like  $\mathbf{P}_v$ , the temporal prompt tokens  $\mathbf{P}_{tmp}$  are also randomly initialized learnable

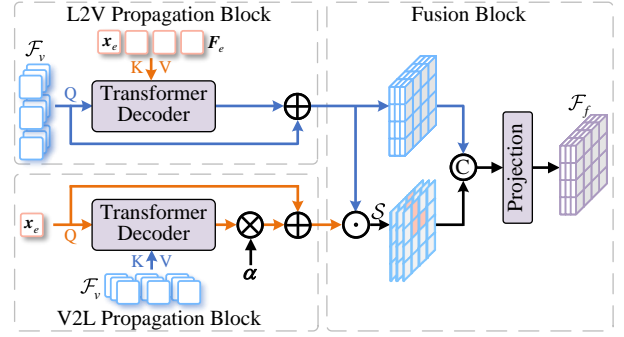


Fig. 6. **Structure of the VL Feature Fusion module,** consisting of a language-to-vision (L2V) propagation block, a vision-to-language (V2L) propagation block, and a fusion block.

vectors. Differently, we adopt a shallow prompt-tuning strategy for the temporal prompt. We repeat  $\mathbf{P}_{tmp}$  for  $T_c$  times and append the  $t$ -th copy  $\mathbf{P}_{tmp}^t$  to the patch embeddings of  $\mathbf{I}^t$  in the first transformer layer. In each layer, we use the output embeddings corresponding to the temporal prompt tokens as carriers for temporal modeling. Specifically, we construct a Parameter-Reusing Temporal Capture (PRTC) module on the output of each vision transformer layer to capture the temporal clue of the video. In the  $l$ -th layer, it takes as input the visual features  $\mathcal{F}_v^l = \{\mathbf{F}_v^{t,l}\}_{t=T}^{T+T_c-1}$  and temporal embeddings  $\hat{\mathcal{P}}_{tmp}^l = \{\hat{\mathbf{P}}_{tmp}^{t,l}\}_{t=T}^{T+T_c-1}$  of all frames, and outputs the new temporal embeddings  $\mathcal{P}_{tmp}^l = \{\mathbf{P}_{tmp}^{t,l}\}_{t=T}^{T+T_c-1}$  modeling the temporal clues. The temporal clues embedded in  $\mathcal{P}_{tmp}^l$  are further spread to the visual features via the interaction of the  $(l+1)$ -th vision transformer layer.

As shown in Figure 5, the PRTC module reuses the frozen visual transformer layer in VLP models as both the encoder and decoder. Technically, we directly replace the MSA operation with the MCA operation to convert an encoder into a decoder. PRTC employs the encoder to perform the interaction between the temporal embeddings of all frames and uses the decoder to perform the interaction between the temporal embeddings and visual features of all frames. The temporal clues are embedded into  $\mathcal{P}_{tmp}^l$  through the aforementioned cross-frame interactions. Denoting the encoder and decoder by  $\Phi_{Enc}^l$  and  $\Phi_{Dec}^l$  in the  $l$ -th layer, the above operation can be formulated as:

$$\mathcal{P}_{tmp}^l = \Phi_{Dec}^l(\Phi_{Enc}^l(\hat{\mathcal{P}}_{tmp}^l, \mathcal{F}_v^l)). \quad (1)$$

**Historical prompt.** VLP-RVOS processes long videos clip-by-clip. Therefore, we introduce historical prompt tokens, conditioned on the target states in the previous clip, to provide historical prior for the VLP model. Technically, each historical prompt token is calculated based on the feature of a previous frame through a masked global pooling layer following a linear projection layer. We adopt a deep prompt-tuning strategy with the historical prompts by appending them to every vision transformer layer. Particularly, we use different linear projection layers to generate the historical prompt tokens for each visual transformer layer, as different layers have different semantic levels.

With the above prompt-tuning method, the processing of the  $t$ -th frame in the  $l$ -th vision transformer layer can be

formulated as:

$$\mathbf{F}_p^{t,l-1} = [\mathbf{F}_v^{t,l-1}, \mathbf{P}_h^{l-1}, \mathbf{P}_v^{l-1}, \mathbf{P}_{tmp}^{t,l-1}], \quad (2)$$

$$\tilde{\mathbf{F}}_p^{t,l-1} = \mathbf{F}_p^{t,l-1} + \phi_{\text{MSA}}(\phi_{\text{LN}}(\mathbf{F}_p^{t,l-1})), \quad (3)$$

$$[\mathbf{F}_v^{t,l}, \mathbf{P}_h^l, \mathbf{P}_v^l, \hat{\mathbf{P}}_{tmp}^{t,l}] = \phi_{\text{FFN}}(\phi_{\text{LN}}(\tilde{\mathbf{F}}_p^{t,l-1})) + \tilde{\mathbf{F}}_p^{t,l-1}, \quad (4)$$

where  $\phi_{\text{LN}}$ ,  $\phi_{\text{MSA}}$ , and  $\phi_{\text{FFN}}$  refer to layer normalization, multi-head self-attention, and feed-forward network in the vision transformer layer.

2) *Language prompt-tuning*: Language prompt-tuning aims to adapt the pre-trained language encoder for a comprehensive understanding of the referring expression. We append a set of language prompt tokens  $\mathbf{P}_e \in \mathbb{R}^{m_e \times C_e}$  to the tokenized word embeddings. These tokens can learn the overall distribution of the referring expression data, and facilitate the language encoder modeling textual contexts to understand the referring expression.

Similar to [57], we adopt a transformer encoder to perform the multi-modality prompt interaction before feeding them into the encoders, allowing for the joint learning of multi-modality prompts, as shown in Figure 4.

### C. Reference-guided visual encoding

Unlike many RVOS methods [7], [21] performing VL relation modeling only after feature extraction, we propose to inject the linguistic reference information into the visual encoder during feature extraction, serving as the first stage of VL relation modeling. As shown in Figure 4, we feed the language feature  $\mathbf{F}_e$  into each vision transformer layer and calculate the cross-attention between  $\mathbf{F}_e$  and the visual embeddings of each layer. To this end, we introduce a Multi-head Cross-Attention (MCA) operation in each vision transformer layer, which reuses the parameter of the existing MSA operation. Owing to the alignment nature between the visual and linguistic features, such a simple parameter-reusing MCA operation can effectively modulate the visual feature with the linguistic concept. The formulation of the attention operation in the  $l$ -th layer, *i.e.*, Eqn. 3, is modified as follows:

$$\tilde{\mathbf{F}}_p^{t,l-1} = \mathbf{F}_p^{t,l-1} + \phi_{\text{MSA}}(\phi_{\text{LN}}(\mathbf{F}_p^{t,l-1})) + \phi_{\text{MCA}}(\phi_{\text{LN}}(\mathbf{F}_p^{t,l-1}), \phi_{\text{LN}}(\mathbf{F}_e)), \quad (5)$$

where  $\phi_{\text{MCA}}$  denotes multi-head cross-attention.

### D. VL feature fusion

The VL Feature Fusion (VLFF) module, built on the deep VL feature  $\mathcal{F}_v$  and  $\mathbf{F}_e$ , is used to associate high-level visual semantics with abstract linguistic concepts. As shown in Figure 6, it consists of a vision-to-language (V2L) propagation block, a language-to-vision (L2V) propagation block, and a fusion block. The V2L propagation block uses the global linguistic representation  $\mathbf{x}_e$  as the query to calculate MCA with  $\mathcal{F}_v$ , enhancing the linguistic concepts in  $\mathbf{x}_e$  relevant to the visual content. The L2V propagation block uses  $\mathcal{F}_v$  as the query to calculate MCA with the word-level linguistic feature  $\mathbf{F}_e$ , enhancing the referred visual contents in  $\mathcal{F}_v$ . Herein skip connections are introduced for feature stability. Similar to [58], we rescale the decoder output in the V2L propagation block

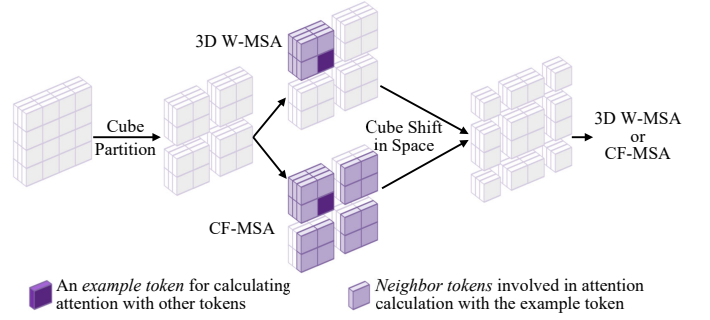


Fig. 7. **Comparison of CF-MSA and 3D W-MSA [9]**. For each token, CF-MSA calculates its attention with its neighbors, including those belonging to the same frame or the same cube. By contrast, 3D W-MSA only calculates the attention within the 3D window. Note that we omit the window partition in the temporal dimension for 3D W-MSA.

using a learnable factor  $\alpha \in \mathbb{R}^{C_e}$  with small initial values to preserve VL alignment.

With the enhanced VL features, VLFF calculates the pixel-wise cosine similarity between them, obtaining the similarity vectors  $\mathcal{S} = \{s^t \in \mathbb{R}^{N_v}\}_{t=T}^{T+T_c-1}$ . After reshaping the enhanced visual features and similarity vectors, we concatenate them frame-by-frame for fusion. Finally, we use a projection layer to reduce the dimension of the fusion feature to  $C$ . We denote the fusion feature by  $\mathcal{F}_f$ .

### E. Spatial-temporal reasoning

The Spatial-Temporal Reasoning (STR) module aims to capture the dynamic vision contents (such as motions and appearance variations) related to the referring expression. As shown in Figure 4, it consists of the spatial-temporal encoder and the transformer decoder, which are used to model the spatial-temporal and vision-language relations, respectively, and repeated for  $N$  times.

We devise a Cube-Frame Multi-head Self-Attention (CF-MSA) mechanism tailored for efficient and effective spatial-temporal encoding, as illustrated in Figure 7. Given the input features  $\mathcal{F}_f \in \mathbb{R}^{T_c \times H \times W \times C}$ , we first partition it into non-overlap cubes (*i.e.*, 3D windows). For each token, we calculate its attention with itself and neighbor tokens belonging to the same frame as well as the same cube. Inspired by [9], [59], we shift the cube in space dimensions and recalculate attention within cubes again for cross-cube modeling. Compared with 3D SW/W-MSA proposed in [9] that models the spatial-temporal relations within 3D windows, CF-MSA further considers the intra-frame global spatial relation, which benefits for perceiving the target location more robustly and accurately. Compared with global MSA, CF-MSA omits the relation between two tokens which are across long distances in both space and time. Assuming the cube size is  $T_c \times M_w \times M_w$ , the computation complexity of the global MSA, 3D W-MSA, and our CF-MSA (without cube shift) operations<sup>1</sup> on  $\mathcal{F}_f \in \mathbb{R}^{T_c \times H \times W \times C}$  are  $\Omega(\text{MSA}) = 2(T_c HW)^2 C$ ,  $\Omega(\text{3D W-MSA}) = 2M_w^2 T_c^2 HWC$ , and  $\Omega(\text{CF-MSA}) = 2T_c HW((T_c - 1)M_w^2 + HW)C$ , respectively.

<sup>1</sup>Linear Projection and SoftMax are omitted in determining complexity.

TABLE I  
EXPERIMENTAL RESULTS ON REF-YOUTUBE-VOS AND REF-DAVIS17.

Algorithms	Visual Backbone	Ref-YouTube-VOS			Ref-DAVIS17		
		$\mathcal{J}\&\mathcal{F}$ (%)	$\mathcal{J}$ (%)	$\mathcal{F}$ (%)	$\mathcal{J}\&\mathcal{F}$ (%)	$\mathcal{J}$ (%)	$\mathcal{F}$ (%)
<i>Trained on Ref-Youtube-VOS alone</i>							
MTTR [6]	Video-Swin-T	55.3	54.0	56.6	–	–	–
MANet [20]	Video-Swin-T	55.6	54.8	56.5	–	–	–
ReferFormer [7]	Video-Swin-T	56.0	54.8	57.3	55.8	51.8	59.8
SgMg [60]	Video-Swin-T	58.9	57.7	60.0	56.7	53.3	60.0
SOC [61]	Video-Swin-T	59.2	57.8	60.5	59.0	55.4	62.6
<b>Ours</b> (CLIP)	ViT-B/16	59.7	57.9	61.5	60.3	56.7	64.0
<b>Ours</b> (CLIP)	ViT-L/14	<u>62.2</u>	<u>60.2</u>	<u>64.3</u>	<u>64.8</u>	<u>61.7</u>	<u>67.9</u>
<b>Ours</b> (VLMo)	VLMo-B/16	60.1	58.4	61.8	61.2	57.3	65.1
<b>Ours</b> (VLMo)	VLMo-L/16	<b>63.3</b>	<b>61.1</b>	<b>65.5</b>	<b>66.5</b>	<b>61.9</b>	<b>71.1</b>
<i>Pre-trained on Ref-COCO+/g and fine-tuned on Ref-Youtube-VOS</i>							
R2VOS [3]	Video-Swin-T	61.3	59.6	63.1	–	–	–
ReferFormer [7]	Video-Swin-T	59.4	58.0	60.9	59.7	56.6	62.8
ReferFormer [7]	Swin-L	62.4	60.8	64.0	60.5	57.6	63.4
ReferFormer [7]	Video-Swin-B	62.9	61.3	64.6	61.1	58.1	64.1
VL [62]	Video-Swin-B	63.8	61.9	65.6	61.6	58.9	64.3
TCAD [31]	Video-Swin-B	65.8	63.6	68.0	64.6	61.6	67.6
HTML [30]	Swin-L	63.4	61.5	65.3	61.6	58.9	64.4
HTML [30]	Video-Swin-B	63.4	61.5	65.2	62.1	59.2	65.1
OnlineRefer [27]	Swin-L	63.5	61.6	65.5	64.8	61.6	67.7
OnlineRefer [27]	Video-Swin-B	62.9	61.0	64.7	62.4	59.1	65.6
RefSAM [63]	ViT-L	62.1	60.9	63.3	<u>68.5</u>	<u>65.2</u>	<u>71.9</u>
SgMg [60]	Video-Swin-B	65.7	63.9	67.4	63.3	60.6	66.0
SOC [61]	Video-Swin-B	<u>66.0</u>	<u>64.1</u>	67.9	64.2	61.0	67.4
<b>Ours</b> (CLIP)	ViT-B/16	62.9	61.3	64.4	65.1	61.4	68.8
<b>Ours</b> (CLIP)	ViT-L/14	<u>66.0</u>	63.6	<u>68.3</u>	68.2	64.6	71.8
<b>Ours</b> (VLMo)	VLMo-B	<u>63.1</u>	61.5	64.7	65.5	60.7	69.4
<b>Ours</b> (VLMo)	VLMo-L	<b>67.6</b>	<b>65.3</b>	<b>69.8</b>	<b>70.2</b>	<b>66.3</b>	<b>74.1</b>

The transformer decoder in STR models the relation between the shallow visual features and the linguistic feature, constituting the third stage of VL relation modeling. It introduces additional low-level semantic guidance from the shallow features, facilitating STR to understand the variations of the visual contents within a video clip.

#### IV. EXPERIMENTS

##### A. Experimental settings

**Datasets and metrics.** We evaluate VLP-RVOS on Ref-Youtube-VOS [18], Ref-DAVIS17 [17], A2D-Sentences [16], and JHMDB-Sentences [16]. For Ref-Youtube-VOS and Ref-DAVIS17, region similarity  $\mathcal{J}$ , contour accuracy  $\mathcal{F}$ , and their average value  $\mathcal{J}\&\mathcal{F}$  are used as metrics, following [18]. For A2D/JHMDB-Sentences, mAP, overall IoU, and mean IoU are used as metrics, following [16].

**Implementation details.** We test our algorithm using different VLP models, including ViT-B/16 CLIP, ViT-L/14 CLIP [11], VLMo-B, and VLMo-L [12].  $C$  is set to 256 to reduce computation complexity.  $N$  is set to 4. We use the features from the 3<sup>rd</sup>, 7<sup>th</sup>, and 9<sup>th</sup> layers for skip connections when ViT-B/16 CLIP or VLMo-B serves as the backbone which contains 12 visual transformer layers, and we use those from the 6<sup>th</sup>, 14<sup>th</sup>, and 18<sup>th</sup> layers for skip connections when ViT-L/14 CLIP or VLMo-L serves as the backbone which contains 24 visual transformer layers.

During training, we freeze the VLP model and optimize the remaining parameters using AdamW [64] with a weight

decay of  $5 \times 10^{-4}$  and a learning rate of  $5 \times 10^{-5}$ . Specifically, for Ref-Youtube-VOS, we train the model on its training set alone and report results on its val set. We also try to pre-train our model on Ref-COCO+/g [65], [66] and fine-tune it on Ref-Youtube-VOS, similar to [3], [7], [23]. For Ref-DAVIS17, we directly report the results of the models trained on Ref-Youtube-VOS, providing insights into cross-dataset generalization. For A2D/JHMDB-Sentences, we train our model on the A2D-Sentences training set alone following [16]. We use the Dice [67] and Focal [68] losses for end-to-end training, whose weights are tuned to be 5 and 2, respectively. For image training data [65], [66], we set  $T_c$  to 1, similar to [7]. For video training data [16]–[18], we set  $T_c$  to 6 and train our model with two consecutive clips sampled from the same videos for each iteration. Thus we can generate historical prompts from the former clip and feed them into the model when performing forward propagation on the latter clip. This training strategy enables our VLP-RVOS to learn to exploit the historical prior. During inference,  $T_c$  is set to 6 by default to maintain consistency with the training settings. Besides, we directly output the predicted masks without post-processing. We will release our source codes.

##### B. Comparison with state-of-the-art methods

**Ref-Youtube-VOS & Ref-DAVIS17.** Table I reports the experimental results on Ref-Youtube-VOS and Ref-DAVIS17. The models are divided into two groups based on the training protocol. Our model with VLMo-L achieves the best perfor-

TABLE II  
EXPERIMENTAL RESULTS ON A2D/JHMDB-SENTENCES. † DENOTES THAT THE MODEL IS ADDITIONALLY PRE-TRAINED ON REF-COCO+/G BEFORE BEING TRAINED ON A2D-SENTENCES.

Algorithms	Visual Backbone	A2D-Sentences			JHMDB-Sentences		
		mAP (%)	IoU <sub>Overall</sub> (%)	IoU <sub>Mean</sub> (%)	mAP (%)	IoU <sub>Overall</sub> (%)	IoU <sub>Mean</sub> (%)
ReferFormer† [7]	Video-Swin-B	55.0	78.6	70.3	43.7	73.0	71.8
SOC† [61]	Video-Swin-B	57.3	80.7	72.5	44.6	73.6	72.3
SgMg† [60]	Video-Swin-B	58.5	79.9	72.0	45.0	73.7	72.5
LBDT-4 [4]	ResNet-50	47.2	70.4	62.1	41.1	64.5	65.8
TCAD [31]	ResNet-50	–	76.6	68.6	–	70.6	69.6
LoSh-R [69]	Video-Swin-T	50.4	74.3	66.6	40.7	71.6	71.3
SOC [61]	Video-Swin-T	50.4	74.7	66.9	39.7	70.7	70.1
ReferFormer [7]	Video-Swin-S	53.9	77.7	69.8	42.4	72.8	71.5
OnlineRefer [27]	Video-Swin-B	–	79.6	70.5	–	73.5	71.9
<b>Ours</b> (CLIP)	ViT-B/16	53.3	76.7	69.5	44.2	73.6	71.9
<b>Ours</b> (CLIP)	ViT-L/14	59.4	84.0	75.3	46.0	77.9	75.9
<b>Ours</b> (VLMo)	VLMo-B	53.9	78.5	72.7	44.6	73.7	72.3
<b>Ours</b> (VLMo)	VLMo-L	<b>63.1</b>	<b>86.2</b>	<b>77.7</b>	<b>47.1</b>	<b>78.3</b>	<b>76.6</b>

TABLE III  
FLOPS, SPEED, AND  $\mathcal{J}\&\mathcal{F}$ . WE MEASURE FLOPS AND SPEED OVER REF-YOUTUBE-VOS ON RTX3090. LONG VIDEOS ARE DROPPED TO AVOID GPU MEMORY OVERFLOW. THE MODELS ARE PRE-TRAINED ON REF-COCO+/G AND FINE-TUNED ON REF-YOUTUBE-VOS.

Algorithms	Visual Backbone	Inference Clip Length	FLOPs per frame (G)	Speed (FPS)	$\mathcal{J}\&\mathcal{F}$ (%)	
					Ref-Youtube-VOS	Ref-DAVIS17
ReferFormer [7]	Video-Swin-T	all video frames	72	59	59.4	59.6
ReferFormer [7]	Video-Swin-B	all video frames	132	35	62.9	61.1
ReferFormer [7]	Swin-L	all video frames	220	37	62.4	60.5
SgMg [60]	Video-Swin-T	all video frames	65	67	62.0	61.9
SgMg [60]	Video-Swin-B	all video frames	121	41	65.7	63.3
SOC [61]	Video-Swin-T	all video frames	43	64	62.4	63.5
SOC [61]	Video-Swin-B	all video frames	98	34	66.0	64.2
OnlineRefer [27]	Swin-L	1	222	11	63.5	64.8
<b>Ours</b> (CLIP)	ViT-B/16	6 (our default setting)	72	77	62.9	65.1
<b>Ours</b> (CLIP)	ViT-L/14	6 (our default setting)	219	30	66.0	68.2
<b>Ours</b> (VLMo)	VLMo-B	6 (our default setting)	61	55	63.1	65.5
<b>Ours</b> (VLMo)	VLMo-L	6 (our default setting)	183	22	67.6	70.2
<b>Ours</b> (CLIP)	ViT-B/16	all video frames	71	103	62.8	64.5
<b>Ours</b> (CLIP)	ViT-L/14	all video frames	202	36	65.9	67.9
<b>Ours</b> (VLMo)	VLMo-B	all video frames	58	70	62.8	65.1
<b>Ours</b> (VLMo)	VLMo-L	all video frames	173	29	67.4	70.0

mance in all metrics in both groups on the two benchmarks. Compared with ReferFormer (Swin-L), HTML (Swin-L), OnlineRefer (Swin-L), and RefSAM (ViT-L), which also use the backbone pre-trained on images, our methods with ViT-L/14 or VLMo-L as the visual backbone improve the segmentation performance with substantial margins, demonstrating the effectiveness of our VLP-RVOS. Besides, our methods perform favorably against state-of-the-art methods using the backbone pre-trained on videos, which manifests the potential of our temporal modeling approach.

Besides, compared with other models, most of our models exhibit substantial advantages in cross-dataset evaluation, *i.e.*, training on Ref-Youtube-VOS and testing on Ref-DAVIS17. For example, VLP-RVOS with VLMo-B and VLMo-L improves the performance by 1.3% and 6.0% in  $\mathcal{J}\&\mathcal{F}$  on Ref-DAVIS17, respectively, compared with SOC which using Video-Swin-B as the backbone. The cross-dataset evaluation results highlight the strong generalization ability of our VLP-RVOS.

**A2D-Sentences & JHMDB-Sentences.** Table II presents the experimental results on the A2D-Sentences and JHMDB-Sentences datasets. Our methods using ViT-B/14 CLIP and VLMo-B perform favorably against recently proposed methods, including SOC [61], OnlineRefer [27], and ReferFormer [7]. Our algorithms using ViT-L/14 CLIP and VLMo-L outperform these models by large margins, even those additionally pre-trained on Ref-COCO+/g.

**Efficiency.** Table III reports FLOPs, speeds, and  $\mathcal{J}\&\mathcal{F}$ . Our models with default setting ( $T_c = 6$ ) achieve real-time or near real-time speeds. Inference clip length  $T_c$  also influences efficiency and performance. By setting  $T_c$  to the video length like other algorithms, our VLP-RVOS can run much faster without obviously compromising segmentation performance. For example, VLP-RVOS with ViT-B/16 CLIP runs at 103 FPS with a  $\mathcal{J}\&\mathcal{F}$  score of 62.8. Compared to other models with *similar speeds*, our models show comparable or superior performance on Ref-Youtube-VOS and Ref-DAVIS17, demonstrating the potential of applying VLP models to RVOS.

TABLE IV

ABLATION STUDIES OF EACH COMPONENT ON REF-YOUTUBE-VOS. LP, VP, TP, AND HP DENOTE THE LANGUAGE PROMPT, VISION PROMPT, TEMPORAL PROMPT, AND HISTORICAL PROMPT, RESPECTIVELY. STAGE-1/2/3 DENOTES THE THREE VL RELATION MODELING STAGES. THE BEST AND SECOND-BEST RESULTS ARE MARKED IN BOLD AND UNDERLINE, RESPECTIVELY.

	Prompt-tuning			VL relation modeling			CF-MSA	Spatial-temporal encoder			$\mathcal{J}\&\mathcal{F}$ (%)
	LP+VP	TP	HP	Stage-1	Stage-2	Stage-3		Global MSA	3D W-MSA		
1)	×	×	×	×	×	✓	×	×	×	47.9	
2)	✓	×	×	×	×	✓	×	×	×	51.8	
3)	✓	✓	×	×	×	✓	×	×	×	54.1	
4)	✓	✓	✓	×	×	✓	×	×	×	54.9	
5)	✓	✓	✓	✓	×	✓	×	×	×	56.3	
6)	✓	✓	✓	×	✓	✓	×	×	×	56.0	
7)	✓	✓	✓	✓	✓	✓	×	×	×	57.5	
8)	✓	✓	✓	✓	✓	✓	✓	×	×	<b>59.7</b>	
9)	✓	✓	✓	✓	✓	✓	×	✓	×	58.4	
10)	✓	✓	✓	✓	✓	✓	×	×	✓	<u>58.5</u>	

TABLE V

COMPARISONS OF DIFFERENT ADAPTATION AND TEMPORAL MODELING METHODS OVER OUR VLP-RVOS FRAMEWORK. FULL FINE-TUNING MEANS FINE-TUNING THE ENTIRE VISION ENCODER. PARTIAL- $m$  MEANS FINE-TUNING ONLY THE LAST  $m$  LAYERS OF THE VISION ENCODER. PRTC DENOTES THE PARAMETER-REUSING TEMPORAL CAPTURING MODULE.  $\mathcal{J}\&\mathcal{F}$  IS REPORTED.

	Adaptation					Prompt-tuning (Ours)	Temporal modeling		
	Frozen	Partial-1	Partial-3	Full fine-tuning	Adapter-tuning		TeViT [70]	IFC [71]	PRTC (Ours)
Ref-Youtube-VOS	54.3	55.1	<u>58.5</u>	56.8	58.0	<b>59.7</b>	57.6	<u>58.2</u>	<b>59.7</b>
Ref-DAVIS17	<u>58.2</u>	57.1	55.1	53.5	58.1	<b>60.3</b>	58.2	<u>58.8</u>	<b>60.3</b>

### C. Ablation studies

In our ablation experiments, We use ViT-B/16 CLIP [11] as the VLP model and train all the variants on the Ref-Youtube-VOS training set alone.

1) *Analyses on proposed components.*: We analyze the proposed components through 10 variants, as shown in Table IV. The experiments begin with a baseline (Variant-1) consisting of a frozen VLP model,  $N$  transformer decoder layers originally used for stage-3 VL relation modeling, and a segmentation head.

**Analyses on temporal-aware VL prompt-tuning.** We gradually introduce different prompts into the baseline to analyze their effect (Variant-2/3/4). The language and vision prompts enable Variant-2 to adapt pre-trained representations for pixel-level prediction, improving  $\mathcal{J}\&\mathcal{F}$  by 3.9%. By introducing the temporal prompts (3,072 learnable parameters) and the PRTC module (no learnable parameters), Variant-3 improves  $\mathcal{J}\&\mathcal{F}$  by 2.3%. It shows that a few learnable parameters effectively enhance the temporal modeling ability. The performance gap between Variant-3 and Variant-4 indicates that historical prompts benefit RVOS in the clip-by-clip inference paradigm.

**Analyses on multi-stage VL relation modeling.** We introduce the first two stages of VL relation modeling into Variant-4 to analyze our multi-stage VL relation modeling scheme (Variant-5/6/7). The comparisons between Variant-4/5/6/7 manifest that both Stage-1 and Stage-2 contribute to a stronger VL understanding ability, and integrating the three stages further improves RVOS performance.

**Analyses on spatial-temporal attention.** We construct Variant-8/9/10 modeling the dense spatial-temporal relation with our CF-MSA, global MSA, and 3D SW/W-MSA [9],

respectively. Compared with Variant-7 which only models the temporal clue by the vision encoder, all the attention mechanisms bring performance gains, demonstrating the necessity of explicit spatial-temporal relation modeling. Besides, CF-MSA achieves the largest performance gain of 2.2%, demonstrating its effectiveness.

2) *Analyses on adaptation methods.* We conduct experiments with several popular adaptation methods on VLP-RVOS to analyze their effect. The involved methods include: 1) Frozen, in which the VLP model is frozen; 2) Partial- $m$ , in which the last  $m$  layers of the vision encoder are fine-tuned; 3) Full fine-tuning, in which the entire vision encoder is fine-tuned (note that the language encoder is kept frozen following [7], [15], [27]); 4) Adapter-tuning, in which additional MLP layers are introduced to tune pre-trained representations. We use UniAdapter [72], which has proven to be effective on several cross-modality tasks.

We report the within-dataset (Ref-Youtube-VOS) and cross-dataset (Ref-DAVIS17) evaluation results in Table V. Although the frozen method obtains the worst performance on Ref-Youtube-VOS, it performs well on Ref-DAVIS17 as it retains the pre-trained knowledge. Compared with partial fine-tuning, full fine-tuning cannot obtain better performance and even harm generalization. UniAdapter [72] obtains mediocre performance. We speculate the reason is that it is designed for image-level VL understanding. Our prompt-tuning performs best on the two benchmarks, demonstrating its effectiveness and generalization.

3) *Analyses on temporal modeling methods.* We conduct experiments with two popular methods, TeViT [70] and IFC [71], which are also designed for temporal modeling within vision transformers. TeViT [70] shifts several learn-



TABLE VI  
EXPERIMENTAL RESULTS OF CROSS-USING VLP MODELS AND APPLYING CLIP TO OTHER RVOS FRAMEWORKS. ALL MODELS ARE TRAINED ON REF-YOUTUBE-VOS ALONE.

Algorithms	Pre-trained Vision Encoder	Pre-trained Language Encoder	Aligned VL Space	$\mathcal{J}\&\mathcal{F}$ (%)	
				Ref-Youtube-VOS	Ref-DAVIS17
Ours (CLIP)	CLIP ViT-B/16	CLIP BERT	✓	<u>59.7</u>	<u>60.3</u>
Ours (VLMO)	VLMO-B Vision Encoder	VLMO-B Language Encoder	✓	<b>60.1</b>	<b>61.2</b>
Ours (CLIP-VLMO)	CLIP ViT-B/16	VLMO-B Language Encoder	✗	55.7	52.2
Ours (VLMO-CLIP)	VLMO-B Vision Encoder	CLIP BERT	✗	54.8	50.5
ReferFormer [7]	Video-Swin-T	RoBERTa	✗	56.0	55.8
ReferFormer [7]+CLIP	CLIP ViT-B/16	CLIP BERT	✓	51.8 (-4.2)	51.1 (-4.7)
SgMg [60]	Video-Swin-T	RoBERTa	✗	58.9	56.7
SgMg [60]+CLIP	CLIP ViT-B/16	CLIP BERT	✓	52.7 (-6.2)	51.9 (-4.8)

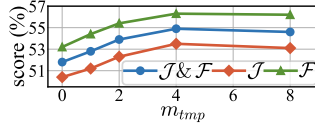
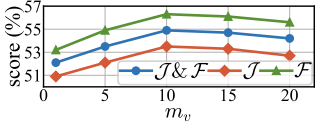


Fig. 8. Experimental results with varying visual/language prompt token numbers (left) and temporal prompt token numbers (right).

able tokens across frames for temporal modeling. IFC [71] introduces a trainable transformer encoder for temporal aggregation, introducing 66 M learnable parameters. We evaluate the two methods in VLP-RVOS and report the results in Table V. The comparisons demonstrate the superiority of our PRTC. Moreover, PRTC occupies a small proportion of the computational load during the visual encoding process. For instance, the total FLOPs per frame for visual encoding with VLMO-L amount to approximately 152.2G, whereas for PRTC, it is only 1.9G.

4) *Effect of the prompt token number:* We conduct studies on the number of vision/language prompt tokens ( $m_v$  and  $m_e$ ) and the number of temporal prompt tokens ( $m_{tmp}$ ) based on Variant-4. We directly set  $m_e = m_v$  to narrow the hyper-parameter search space. As shown in Figure 8, the performance improves along with  $m_v$  and  $m_{tmp}$  increasing and saturates at 10 and 4, respectively.

5) *Effect of the aligned VL space and our transferring framework:* We delve deeper into analyses by breaking the aligned VL space and applying CLIP to other RVOS frameworks. We break the aligned VL space by cross-using the vision and language encoders of CLIP and VLMO, which results in significant performance drops, as shown in Table VI. We also integrate CLIP into ReferFormer and SgMg, where we follow [73] to obtain hierarchical features based on ViT. Table VI shows that applying CLIP to ReferFormer or SgMg leads to large performance drops. These results highlight that both the aligned VL space and our transferring framework are crucial for achieving state-of-the-art performance.

6) *Temporal modeling across different time spans:* As shown in Figure 9, our VLP-RVOS exhibits superior and more consistent performance with varying inference clip lengths, in contrast to ReferFormer which uses a video backbone. The comparisons demonstrate the strong temporal modeling ability of our method.

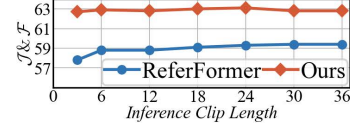


Fig. 9. Experimental results with varying inference clip lengths of ReferFormer (Video-Swin-T) and VLP-RVOS (ViT-B/16 CLIP), which have similar computation complexity. These models are trained on Ref-Youtube-VOS alone.

#### D. Qualitative results

we present qualitative results on several challenging videos to obtain more insights into the pros and cons of VLP-RVOS.

**Comparisons with state-of-the-art methods.** We first qualitatively compare our VLP-RVOS (VLMO-L) with two state-of-the-art algorithms ReferFormer (Video-Swin-B) and SgMg (Video-Swin-B) on two videos. Figure 10 illustrates the segmentation results in a video where the referred objects undergo occlusions. Our VLP-RVOS exhibits superior robustness compared to ReferFormer and SgMg. The favorable performance manifests that the temporal-aware prompt-tuning method and the spatial-temporal reasoning module equip the model with strong temporal modeling ability.

Figure 11 shows the segmentation results in a video with cluttered scenes. Our VLP-RVOS accurately comprehends detailed descriptions and precisely segments the referred objects, whereas ReferFormer and SgMg face difficulties in understanding these complex scenarios. The favorable performance shows that transferring the knowledge of VLP models boosts the vision-language understanding ability of our model.

**Comparison between w/o and w/ temporal prompts.** We qualitatively compare Variant-2 (w/o temporal prompts) and Variant-3 (w/ temporal prompts) to obtain more insights into the effect of the temporal prompt. Figure 12 illustrates their segmentation results over consecutive frames of the same clip on several videos. Note that the videos in Ref-Youtube-VOS are annotated every 5 frames and VLP-RVOS performs segmentation on the annotated frames. We can observe that Variant-3 generates much more stable and consistent segmentation masks across consecutive frames than Variant-2. These comparisons demonstrate the effectiveness of temporal prompts for temporal modeling.

**Comparison between w/o and w/ historical prompts.** We also qualitatively compare Variant-3 (w/o historical prompts) and Variant-4 (w/ historical prompts) to analyze the effect of

Query: *a person's hand picking up a blue switch blade.*  
 Query: *the grey and white knife is behind another sitting on the grey leather.*  
 Query: *a small knife with a blue handle.*

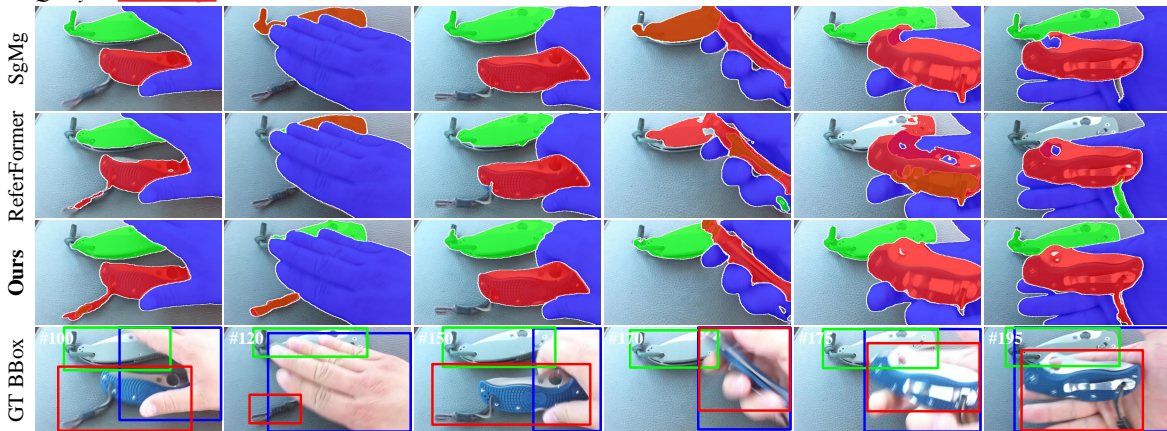


Fig. 10. **Qualitative comparison between VLP-RVOS (VLMo-L), SgMg (Video-Swin-B), and ReferFormer (Video-Swin-B) on a video where a hand is picking up a knife.** All the methods can precisely segment the targets according to the descriptions at the beginning. Nevertheless, when the knives are occluded, SgMg and ReferFormer confuse the two similar knives, leading to erroneous predictions at the 120<sup>th</sup> and 170<sup>th</sup> frames. By contrast, our method is more robust to the occlusion and keeps segmenting the knives precisely.

Query: *the bottle is in front of the paper towels and to the left of the toilet.*  
 Query: *tissue paper near a red bottle.*  
 Query: *the white, green and blue spray bottle is on the bathroom counter and against the mirror.*  
 Query: *a person is explaining something about the basin in the bathroom.*

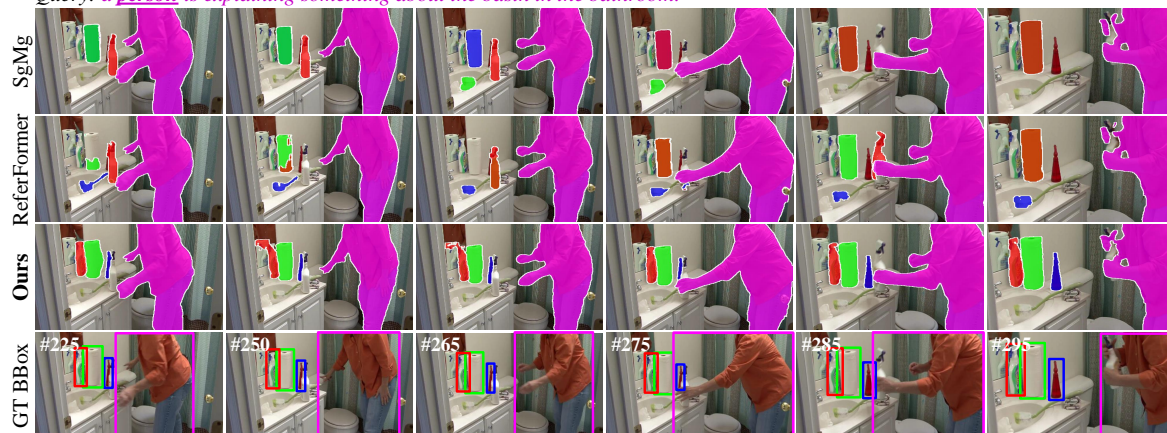


Fig. 11. **Qualitative comparison between VLP-RVOS (VLMo-L), SgMg (Video-Swin-B), and ReferFormer (Video-Swin-B) on a video where some cleaning supplies are placed on the sink.** Our method accurately comprehends the spatial positions and appearances described in the queries, successfully locating these cleaning supplies. In contrast, SgMg and ReferFormer encounter difficulties in understanding the descriptions within this cluttered scene.

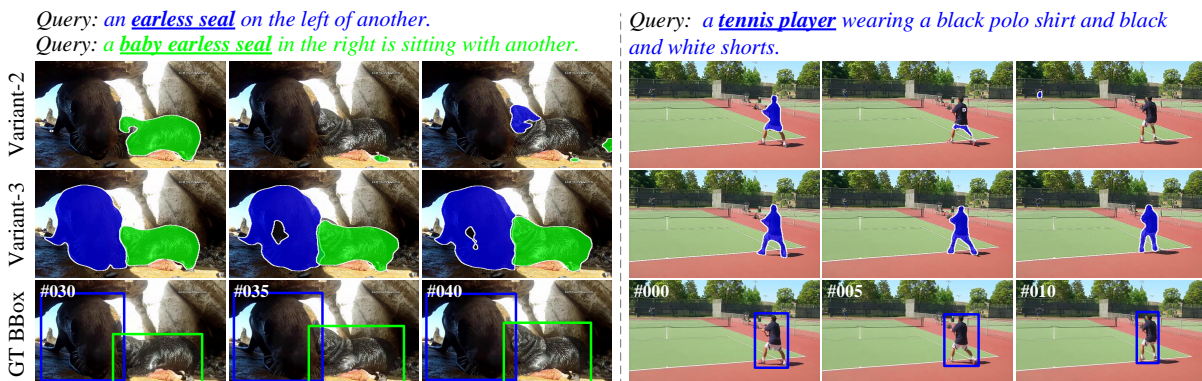


Fig. 12. **Qualitative comparisons between Variant-2 (w/o temporal prompts) and Variant-3 (w/ temporal prompts) on two challenging videos.** For each video, we visualize the prediction results on the consecutive frames of the same clip to analyze the effect of the temporal prompt. Without considering the temporal clues, Variant-2 performs segmentation on each frame independently. Consequently, it predicts inconsistent masks across consecutive frames within a video clip. By contrast, Variant-3 with temporal prompts generates more stable and consistent predictions on consecutive frames.

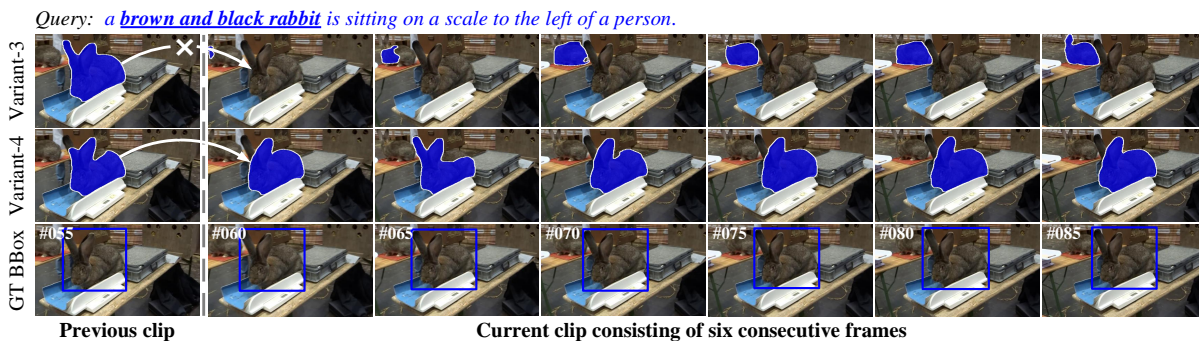


Fig. 13. **Qualitative comparisons between Variant-3 (w/o historical prompts) and Variant-4 (w/ historical prompts) on a challenging video.** The 55<sup>th</sup> frame is from the previous clip, and both Variant-3 and Variant-4 successfully locate the referred rabbit in this frame. With the historical prior of the referred rabbit, Variant-4 keeps tracking it in the current clip (from the 60<sup>th</sup> to the 85<sup>th</sup> frame). By contrast, the segmentation masks of Variant-3 drift to the distractor in the current clip, which is a similar rabbit gradually appearing in the view.

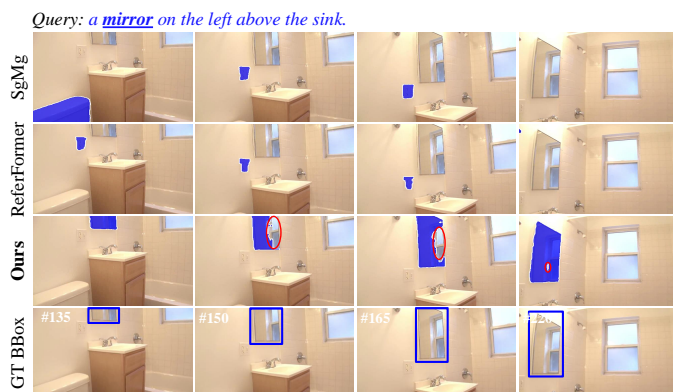


Fig. 14. **Prediction results for segmenting a mirror.** The referred object is a mirror located on the left above the sink. Although being able to understand the concept of the mirror and locate it, VLP-RVOS has difficulty distinguishing between the reflection inside the mirror and the real object outside, as highlighted by the red circles.

the historical prompt. Figure 13 illustrates their segmentation results over two consecutive clips on a video. Both Variant-3 and Variant-4 can locate the referred rabbit in the previous clip (as shown in the 55<sup>th</sup> frame). Nevertheless, Variant-3 loses the referred rabbit and drifts to a distractor in the following clip (from the 60<sup>th</sup> to the 85<sup>th</sup> frame). By contrast, Variant-4 with the target prior from the previous clip continues tracking this rabbit in the following clip.

**Failure cases.** Although VLP-RVOS has shown promising vision-language understanding abilities in the above experiments, we observe a challenge in distinguishing between reflections inside mirrors and real objects outside. As shown in Figure 14, VLP-RVOS can recognize the presence of the mirror, but it incorrectly identifies the reflection inside the mirror as the real object. A potential and straightforward solution is to further enhance the contextual modeling ability and meanwhile incorporate the mirror data [74] for training.

## V. CONCLUSION

We have presented a VLP-RVOS framework to transfer VLP models to RVOS. It enables learning relation modeling for RVOS from aligned VL space instead of from scratch. Specifically, we propose a temporal-aware prompt-tuning method,

which not only adapts pre-trained representations for pixel-level prediction but also empowers the vision encoder to model temporal clues. We further propose a multi-stage VL relation modeling scheme for comprehensive VL understanding. Besides, we design a cube-frame attention mechanism for efficient and effective spatial-temporal reasoning. Extensive experiments on four benchmarks demonstrate the effectiveness and generalization of VLP-RVOS.

## REFERENCES

- [1] S. Liu, T. Hui, S. Huang, Y. Wei, B. Li, and G. Li, “Cross-modal progressive comprehension for referring segmentation,” *IEEE TPAMI*, vol. 44, no. 9, pp. 4761–4775, 2021.
- [2] X. Wang, Q. Huang, A. Celikyilmaz, J. Gao, D. Shen, Y.-F. Wang, W. Y. Wang, and L. Zhang, “Reinforced cross-modal matching and self-supervised imitation learning for vision-language navigation,” in *CVPR*, 2019, pp. 6629–6638.
- [3] X. Li, J. Wang, X. Xu, X. Li, B. Raj, and Y. Lu, “Robust referring video object segmentation with cyclic structural consensus,” in *ICCV*, 2023, pp. 22 236–22 245.
- [4] Z. Ding, T. Hui, J. Huang, X. Wei, J. Han, and S. Liu, “Language-bridged spatial-temporal interaction for referring video object segmentation,” in *CVPR*, 2022, pp. 4964–4973.
- [5] T.-J. Fu, X. E. Wang, S. T. Grafton, M. P. Eckstein, and W. Y. Wang, “M3I: Language-based video editing via multi-modal multi-level transformers,” in *CVPR*, 2022, pp. 10 513–10 522.
- [6] A. Botach, E. Zheltonozhskii, and C. Baskin, “End-to-end referring video object segmentation with multimodal transformers,” in *CVPR*, 2022, pp. 4985–4995.
- [7] J. Wu, Y. Jiang, P. Sun, Z. Yuan, and P. Luo, “Language as queries for referring video object segmentation,” in *CVPR*, 2022, pp. 4974–4984.
- [8] K. He, X. Zhang, S. Ren, and J. Sun, “Deep residual learning for image recognition,” in *CVPR*, 2016, pp. 770–778.
- [9] Z. Liu, J. Ning, Y. Cao, Y. Wei, Z. Zhang, S. Lin, and H. Hu, “Video swin transformer,” in *CVPR*, 2022, pp. 3202–3211.
- [10] Y. Liu, M. Ott, N. Goyal, J. Du, M. Joshi, D. Chen, O. Levy, M. Lewis, L. Zettlemoyer, and V. Stoyanov, “Roberta: A robustly optimized bert pretraining approach,” *arXiv preprint arXiv:1907.11692*, pp. 1–13, 2019.
- [11] A. Radford, J. W. Kim, C. Hallacy, A. Ramesh, G. Goh, S. Agarwal, G. Sastry, A. Askell, P. Mishkin, J. Clark *et al.*, “Learning transferable visual models from natural language supervision,” in *ICML*. PMLR, 2021, pp. 8748–8763.
- [12] H. Bao, W. Wang, L. Dong, Q. Liu, O. K. Mohammed, K. Aggarwal, S. Som, S. Piao, and F. Wei, “Vlmo: Unified vision-language pre-training with mixture-of-modality-experts,” in *NeurIPS*, vol. 35, 2022, pp. 32 897–32 912.
- [13] Z. Wang, Y. Lu, Q. Li, X. Tao, Y. Guo, M. Gong, and T. Liu, “Cris: Clip-driven referring image segmentation,” in *CVPR*, 2022, pp. 11 686–11 695.
- [14] Z. Xu, Z. Chen, Y. Zhang, Y. Song, X. Wan, and G. Li, “Bridging vision and language encoders: Parameter-efficient tuning for referring image segmentation,” in *ICCV*, 2023, pp. 17 503–17 512.

- [15] Y. Rao, W. Zhao, G. Chen, Y. Tang, Z. Zhu, G. Huang, J. Zhou, and J. Lu, "Denseclip: Language-guided dense prediction with context-aware prompting," in *CVPR*, 2022, pp. 18 082–18 091.
- [16] K. Gavriluyk, A. Ghodrati, Z. Li, and C. G. Snoek, "Actor and action video segmentation from a sentence," in *CVPR*, 2018, pp. 5958–5966.
- [17] A. Khoreva, A. Rohrbach, and B. Schiele, "Video object segmentation with language referring expressions," in *ACCV*. Springer, 2019, pp. 123–141.
- [18] S. Seo, J.-Y. Lee, and B. Han, "Urvos: Unified referring video object segmentation network with a large-scale benchmark," in *ECCV*. Springer, 2020, pp. 208–223.
- [19] B. McIntosh, K. Duarte, Y. S. Rawat, and M. Shah, "Visual-textual capsule routing for text-based video segmentation," in *CVPR*, 2020, pp. 9942–9951.
- [20] W. Chen, D. Hong, Y. Qi, Z. Han, S. Wang, L. Qing, Q. Huang, and G. Li, "Multi-attention network for compressed video referring object segmentation," in *ACM MM*, 2022, pp. 4416–4425.
- [21] D. Li, R. Li, L. Wang, Y. Wang, J. Qi, L. Zhang, T. Liu, Q. Xu, and H. Lu, "You only infer once: Cross-modal meta-transfer for referring video object segmentation," in *AAAI*, vol. 36, no. 2, 2022, pp. 1297–1305.
- [22] Z. Ding, T. Hui, S. Huang, S. Liu, X. Luo, J. Huang, and X. Wei, "Progressive multimodal interaction network for referring video object segmentation," *The 3rd Large-scale Video Object Segmentation Challenge*, vol. 8, pp. 1–4, 2021.
- [23] C. Liang, Y. Wu, T. Zhou, W. Wang, Z. Yang, Y. Wei, and Y. Yang, "Rethinking cross-modal interaction from a top-down perspective for referring video object segmentation," *arXiv preprint arXiv:2106.01061*, pp. 1–4, 2021.
- [24] L. Ye, M. Rochan, Z. Liu, and Y. Wang, "Cross-modal self-attention network for referring image segmentation," in *CVPR*, 2019, pp. 10 502–10 511.
- [25] K. Ning, L. Xie, F. Wu, and Q. Tian, "Polar relative positional encoding for video-language segmentation," in *IJCAI*, vol. 9, 2020, pp. 948–954.
- [26] T. Hui, S. Huang, S. Liu, Z. Ding, G. Li, W. Wang, J. Han, and F. Wang, "Collaborative spatial-temporal modeling for language-queried video actor segmentation," in *CVPR*, 2021, pp. 4187–4196.
- [27] D. Wu, T. Wang, Y. Zhang, X. Zhang, and J. Shen, "Onlinerefer: A simple online baseline for referring video object segmentation," in *ICCV*, 2023, pp. 2761–2770.
- [28] X. Hu, B. Hampiholi, H. Neumann, and J. Lang, "Temporal context enhanced referring video object segmentation," in *WACV*, January 2024, pp. 5574–5583.
- [29] N. Carion, F. Massa, G. Synnaeve, N. Usunier, A. Kirillov, and S. Zagoruyko, "End-to-end object detection with transformers," in *ECCV*. Springer, 2020, pp. 213–229.
- [30] M. Han, Y. Wang, Z. Li, L. Yao, X. Chang, and Y. Qiao, "Htm1: Hybrid temporal-scale multimodal learning framework for referring video object segmentation," in *ICCV*, October 2023, pp. 13 414–13 423.
- [31] J. Tang, G. Zheng, and S. Yang, "Temporal collection and distribution for referring video object segmentation," in *ICCV*, 2023, pp. 15 466–15 476.
- [32] G. Feng, L. Zhang, Z. Hu, and H. Lu, "Learning from box annotations for referring image segmentation," *IEEE Transactions on Neural Networks and Learning Systems*, vol. 35, no. 3, pp. 3927–3937, 2024.
- [33] J. Liu, H. Tan, Y. Hu, Y. Sun, H. Wang, and B. Yin, "Global and local interactive perception network for referring image segmentation," *IEEE Transactions on Neural Networks and Learning Systems*, pp. 1–14, 2023.
- [34] J. Yang, L. Zhang, and H. Lu, "Referring image segmentation with fine-grained semantic funneling infusion," *IEEE Transactions on Neural Networks and Learning Systems*, pp. 1–12, 2023.
- [35] W. Wang, T. Yue, Y. Zhang, L. Guo, X. He, X. Wang, and J. Liu, "Unveiling parts beyond objects: Towards finer-granularity referring expression segmentation," *arXiv preprint arXiv:2312.08007*, 2024.
- [36] Z. Yang, J. Wang, Y. Tang, K. Chen, H. Zhao, and P. H. Torr, "Lavt: Language-aware vision transformer for referring image segmentation," in *CVPR*, 2022, pp. 18 155–18 165.
- [37] S. Liu, Y. Ma, X. Zhang, H. Wang, J. Ji, X. Sun, and R. Ji, "Rotated multi-scale interaction network for referring remote sensing image segmentation," *arXiv preprint arXiv:2312.12470*, 2024.
- [38] J. Li, J. Zhang, and D. Tao, "Referring image matting," in *CVPR*, 2023, pp. 22 448–22 457.
- [39] C. Jia, Y. Yang, Y. Xia, Y.-T. Chen, Z. Parekh, H. Pham, Q. Le, Y.-H. Sung, Z. Li, and T. Duerig, "Scaling up visual and vision-language representation learning with noisy text supervision," in *ICML*. PMLR, 2021, pp. 4904–4916.
- [40] X. Li, X. Yin, C. Li, P. Zhang, X. Hu, L. Zhang, L. Wang, H. Hu, L. Dong, F. Wei *et al.*, "Oscar: Object-semantics aligned pre-training for vision-language tasks," in *ECCV*. Springer, 2020, pp. 121–137.
- [41] W. Su, X. Zhu, Y. Cao, B. Li, L. Lu, F. Wei, and J. Dai, "Vi-bert: Pre-training of generic visual-linguistic representations," in *ICLR*, 2020, pp. 1–16.
- [42] J. Lu, D. Batra, D. Parikh, and S. Lee, "Vilbert: Pretraining task-agnostic visiolinguistic representations for vision-and-language tasks," in *NeurIPS*, vol. 32, 2019, pp. 1–11.
- [43] H. Tan and M. Bansal, "Lxmert: Learning cross-modality encoder representations from transformers," *arXiv preprint arXiv:1908.07490*, pp. 1–14, 2019.
- [44] J. Li, D. Li, C. Xiong, and S. Hoi, "Blip: Bootstrapping language-image pre-training for unified vision-language understanding and generation," in *ICML*. PMLR, 2022, pp. 12 888–12 900.
- [45] Y. Zhong, J. Yang, P. Zhang, C. Li, N. Codella, L. H. Li, L. Zhou, X. Dai, L. Yuan, Y. Li *et al.*, "Regionclip: Region-based language-image pretraining," in *Proceedings of the IEEE/CVF Conference on Computer Vision and Pattern Recognition*, 2022, pp. 16 793–16 803.
- [46] N. Ding, Y. Qin, G. Yang, F. Wei, Z. Yang, Y. Su, S. Hu, Y. Chen, C.-M. Chan, W. Chen *et al.*, "Delta tuning: A comprehensive study of parameter efficient methods for pre-trained language models," *arXiv preprint arXiv:2203.06904*, pp. 1–49, 2022.
- [47] Z. Jiang, F. F. Xu, J. Araki, and G. Neubig, "How can we know what language models know?" *TACL*, vol. 8, pp. 423–438, 2020.
- [48] B. Lester, R. Al-Rfou, and N. Constant, "The power of scale for parameter-efficient prompt tuning," in *EMNLP*, 2021, pp. 3045–3059.
- [49] K. Zhou, J. Yang, C. C. Loy, and Z. Liu, "Learning to prompt for vision-language models," *IJCV*, vol. 130, no. 9, pp. 2337–2348, 2022.
- [50] M. Jia, L. Tang, B.-C. Chen, C. Cardie, S. Belongie, B. Hariharan, and S.-N. Lim, "Visual prompt tuning," in *ECCV*. Springer, 2022, pp. 709–727.
- [51] B. Ni, H. Peng, M. Chen, S. Zhang, G. Meng, J. Fu, S. Xiang, and H. Ling, "Expanding language-image pretrained models for general video recognition," in *ECCV*. Springer, 2022, pp. 1–18.
- [52] H. Kwon, T. Song, S. Jeong, J. Kim, J. Jang, and K. Sohn, "Probabilistic prompt learning for dense prediction," in *CVPR*, 2023, pp. 6768–6777.
- [53] S. T. Wasim, M. Naseer, S. Khan, F. S. Khan, and M. Shah, "Vita-clip: Video and text adaptive clip via multimodal prompting," in *CVPR*, 2023, pp. 23 034–23 044.
- [54] C. Ge, R. Huang, M. Xie, Z. Lai, S. Song, S. Li, and G. Huang, "Domain adaptation via prompt learning," *IEEE Transactions on Neural Networks and Learning Systems*, pp. 1–11, 2023.
- [55] A. Dosovitskiy, L. Beyer, A. Kolesnikov, D. Weissenborn, X. Zhai, T. Unterthiner, M. Dehghani, M. Minderer, G. Heigold, S. Gelly *et al.*, "An image is worth 16x16 words: Transformers for image recognition at scale," 2020, pp. 1–21.
- [56] A. Vaswani, N. Shazeer, N. Parmar, J. Uszkoreit, L. Jones, A. N. Gomez, L. Kaiser, and I. Polosukhin, "Attention is all you need," in *NeurIPS*, vol. 30, 2017, pp. 1–11.
- [57] Y. Zang, W. Li, K. Zhou, C. Huang, and C. C. Loy, "Unified vision and language prompt learning," *arXiv preprint arXiv:2210.07225*, pp. 1–13, 2022.
- [58] C. Zhou, C. C. Loy, and B. Dai, "Extract free dense labels from clip," in *ECCV*. Springer, 2022, pp. 696–712.
- [59] Z. Liu, Y. Lin, Y. Cao, H. Hu, Y. Wei, Z. Zhang, S. Lin, and B. Guo, "Swin transformer: Hierarchical vision transformer using shifted windows," in *ICCV*, 2021, pp. 10 012–10 022.
- [60] B. Miao, M. Bennamoun, Y. Gao, and A. Mian, "Spectrum-guided multi-granularity referring video object segmentation," in *ICCV*, 2023, pp. 920–930.
- [61] Z. Luo, Y. Xiao, Y. Liu, S. Li, Y. Wang, Y. Tang, X. Li, and Y. Yang, "Soc: Semantic-assisted object cluster for referring video object segmentation," in *NeurIPS*, vol. 36, 2023, pp. 1–13.
- [62] H. Ding, C. Liu, S. Wang, and X. Jiang, "Vlt: Vision-language transformer and query generation for referring segmentation," *IEEE TPAMI*, vol. 45, no. 6, pp. 7900–7916, 2023.
- [63] Y. Li, J. Zhang, X. Teng, and L. Lan, "Refsam: Efficiently adapting segmenting anything model for referring video object segmentation," *arXiv preprint arXiv:2307.00997*, pp. 1–26, 2023.
- [64] I. Loshchilov and F. Hutter, "Decoupled weight decay regularization," 2019, pp. 1–18.
- [65] L. Yu, P. Poirson, S. Yang, A. C. Berg, and T. L. Berg, "Modeling context in referring expressions," in *ECCV*. Springer, 2016, pp. 69–85.
- [66] J. Mao, J. Huang, A. Toshev, O. Camburu, A. L. Yuille, and K. Murphy, "Generation and comprehension of unambiguous object descriptions," in *CVPR*, 2016, pp. 11–20.

- [67] F. Milletari, N. Navab, and S.-A. Ahmadi, “V-net: Fully convolutional neural networks for volumetric medical image segmentation,” in *3DV. Ieee*, 2016, pp. 565–571.
- [68] T.-Y. Lin, P. Goyal, R. Girshick, K. He, and P. Dollár, “Focal loss for dense object detection,” in *ICCV*, 2017, pp. 2980–2988.
- [69] L. Yuan, M. Shi, and Z. Yue, “Losh: Long-short text joint prediction network for referring video object segmentation,” *arXiv preprint arXiv:2306.08736*, pp. 1–10, 2024.
- [70] S. Yang, X. Wang, Y. Li, Y. Fang, J. Fang, W. Liu, X. Zhao, and Y. Shan, “Temporally efficient vision transformer for video instance segmentation,” in *CVPR*, 2022, pp. 2885–2895.
- [71] S. Hwang, M. Heo, S. W. Oh, and S. J. Kim, “Video instance segmentation using inter-frame communication transformers,” *NeuIPS*, vol. 34, pp. 13 352–13 363, 2021.
- [72] H. Lu, M. Ding, Y. Huo, G. Yang, Z. Lu, M. Tomizuka, and W. Zhan, “Uniadapter: Unified parameter-efficient transfer learning for cross-modal modeling,” *arXiv preprint arXiv:2302.06605*, pp. 1–17, 2023.
- [73] Y. Li, H. Mao, R. Girshick, and K. He, “Exploring plain vision transformer backbones for object detection,” in *ECCV*. Springer, 2022, pp. 280–296.
- [74] X. Yang, H. Mei, K. Xu, X. Wei, B. Yin, and R. W. Lau, “Where is my mirror?” in *ICCV*, 2019, pp. 8809–8818.